In addition to theoretical problems involved with the generation of an ozone hole in October 1958, there is the additional problem of explaining the low Dumont plate measurements in April and May 1958. Heterogeneous reactions on the surfaces of PSCs are necessary for massive losses of ozone, and PSCs form at temperatures below −78°C (*7, 31*). April 1958 temperatures of −60°C are too warm to form PSCs (*19*). It is also possible that chlorine activation may have occurred from the hydrolysis of chlorine nitrate on the sulfate layer. This process requires temperatures below −63°C and a large burden of stratospheric chlorine. Antarctic observations during 1992 indicated elevated levels of OClO beginning in mid-April 1992 as a result of the Pinatubo sulfate layer (*32*). However, although OClO levels were high, ozone levels were near normal. Therefore, even in the presence of both high levels of chlorine and high levels of volcanic aerosols, low ozone at Dumont in April and May 1958 would have been unlikely.

REFERENCES AND NOTES

1. J. B. Farman *et al.*, *Nature* **315**, 207 (1985).
2. S. Chubachi [in *Atmospheric Ozone: Proceedings of the Quadrennial Ozone Symposium*, C. S. Zerefos and A. Ghazi, Eds. (Kluwer, Norwell, MA, 1985), pp. 243–245] also reported low total ozone at Syowa (69°S, 40°E) for October 1982 [prior to the Farman *et al.* paper (*1*)], but he failed to note that these values were abnormal.
3. R. S. Stolarski *et al.*, *Nature* **322**, 308 (1986).
4. See the Antarctic Ozone special issue [*Geophys. Res. Lett.* **13** (no. 12) (1986)].
5. D. Hofmann, paper presented at the American Geophysical Union fall 1993 meeting, San Francisco, CA, 9 December 1993. Preliminary Meteor-3 TOMS total ozone data on 8 October 1993 showed an ozone value of 85 DU near the South Pole.
6. The Airborne Antarctic Ozone Experiment, the National Ozone Expeditions I and II [*J. Geophys. Res.* **94** (nos. D9 and D14) (1989)], and the Upper Atmosphere Research Satellite [*Geophys. Res. Lett.* **20**, 1215–1330 (1993)].
7. Heterogeneous chemical processes on the surfaces of polar stratospheric clouds enhance the chlorine species that can destroy ozone. These chlorine species catalytically destroy ozone to form the ozone hole [J. G. Anderson, D. W. Toohey, W. H. Brune, *Science* **251**, 39 (1991)].
8. G. Dobson, *Appl. Opt.* **7**, 387 (1968).
9. K. Tung, *Geophys. Res. Lett.* **13**, 1308 (1986).
10. The ozone minimum breakdown is discussed in R. Nagatani, *NOAA Tech. Rep. NWS 40* (1988); D. F. Heath *et al.*, *NASA Ref. Publ. 1098* (1982); A. Krueger *et al.*, *NASA Ref. Publ. 1201* (1988); A. Krueger *et al.*, *NASA Ref. Publ. 1225* (1989); and A. Krueger *et al.*, *NASA Ref. Publ. 1264* (1991).
11. P. Rigaud and B. Leroy, *Ann. Geophys.* **11**, 791 (1990).
12. R. Bojkov, *Geophys. Res. Lett.* **13**, 1236 (1986).
13. International Council of Scientific Unions, *Catalogue of Data in the World Centers, 1957–1958* (Pergamon, New York, 1964), Vol. XXXVI, p. 84.
14. D. De Muer [*Ann. Geophys.* **11**, 795 (1990)] commented on the Rigaud and Leroy (*11*) paper, noting that (i) the Dumont variability was substantially larger than other Antarctic sites (notably Halley Bay), (ii) the lack of a correlation of the Dumont data with meteorological data, (iii) the extremely low values of total ozone in early September, and (iv) the rarity of low ozone values (less than 200 DU) at Dumont during the 1980s.
15. D. Hartmann *et al.*, *J. Geophys. Res.* **94**, 16779 (1989).
16. "Ozone Data for the World, November–December 1971 Supplement, IGY/IGC 1957–1959" (Atmospheric and Environmental Services of Canada, World Meteorological Organization, Downsview, Canada, 1971), vol. 12.
17. J. Farman and R. Hamilton, *Br. Antarct. Surv. Sci. Rep. 90* (1975).
18. *World Meteorological Organization Global Ozone Research and Monitoring Project Rep. 20* (1989); W. Komhyr *et al.*, in *Ozone in the Atmosphere: Proceedings of the Quadrennial Ozone Symposium*, R. Bojkov and P. Fabian, Eds. (Deepak, Hampton, VA, 1990), p. 28; P. McCormick and J. Larsen, *Geophys. Res. Lett.* **13**, 1280 (1989); D. Hofmann and S. Oltmans, *J. Geophys. Res.* **98**, 18555 (1993).
19. J. Alt *et al.*, *IGY Gen. Rep. Ser.* **4**, 1 (1959).
20. G. Dobson *et al.* [*Proc. R. Soc. London Ser. A* **122**, 456 (1928)] first showed the relationship of meteorological observations to total ozone. E. Farkas [*N. Zealand J. Sci.*, 386 (1970)] and P. Newman and W. Randel [*J. Geophys. Res.* **93**, 12585 (1988)] both showed the very tight linear spatial correlation of stratospheric temperatures and total ozone over Antarctica. They found that warm lower stratospheric temperatures were related to high total column ozone, whereas low temperatures were correlated with low ozone. Y. Sekiguchi [*Geophys. Res. Lett.* **13**, 1202 (1986)] used the Syowa station data to show that years with low (high) total ozone in October and November are related to cold (warm) lower stratospheric temperatures.
21. Every year of available meteorological data has shown this tight linear relation of total ozone to lower stratospheric temperatures, which is directly related to the adiabatic compression of air; see K. Tung and H. Yang, *J. Geophys. Res.* **93**, 11123 (1988); (*9*).
22. M. Schoeberl *et al.*, *Geophys. Res. Lett.* **13**, 1217 (1986).
23. G. Bluth *et al.*, *ibid.* **19**, 151 (1992).
24. T. Simkin *et al.*, *Volcanoes of the World: A Regional Directory, Gazetteer, and Chronology of Volcanism During the Last 10,000 Years* (Hutchinson Ross, Stroudsberg, PA, 1981).
25. W. G. Mankin and T. M. Coffey, *Science* **226**, 170 (1984).
26. "Atmospheric Ozone 1985," *World Meteorological Organization Global Ozone Research and Monitoring Project Rep. 16* (1985).
27. W. Mankin *et al.*, *Geophys. Res. Lett.* **19**, 179 (1992).
28. H. Johnston [*J. Geophys. Res.* **94**, 18485 (1989)] showed that there was little transport of ^{14}C from Northern Hemisphere atmospheric nuclear tests to the Southern Hemisphere.
29. M. Sato *et al.*, *J. Geophys. Res.* **98**, 22987 (1993); H. Lamb, *Philos. Trans. R. Soc. London* **266**, 425 (1970).
30. R. Rood, *Geophys. Res. Lett.* **13**, 1244 (1986).
31. M. McCormick *et al.*, *Geophys. Res. Lett.* **17**, 381 (1990).
32. S. Solomon *et al.*, *Nature* **363**, 245 (1993).
33. Thanks to G. Labow and E. Hare for supplying the Dobson and Vassey data and to M. Schoeberl, R. Stolarski, J. Gleason, J. Herman, A. Aiken, R. McPeters, J. Miller, B. Mankin, S. Rowland, J. DeLuisi, and G. Bluth for helpful discussion.

24 November 1993; accepted 15 March 1994

Strontium Isotopic Composition of Mid-Cretaceous Seawater

B. Lynn Ingram, Rodolfo Coccioni, Alessandro Montanari,
Frank M. Richter

The ^{87}Sr/^{86}Sr ratio in fish teeth separated from mid-Cretaceous marl and black shale from the northeastern Apennines and Venetian Alps (Italy) define three periods of low ^{87}Sr/^{86}Sr ratio at 121 to 124 million years ago (Ma), 110 to 115 Ma, and 89 to 91 Ma. The ^{87}Sr/^{86}Sr excursions correspond to oceanic anoxic events represented by the Livello Selli, Livello 113, Livello Urbino, and Livello Bonarelli black shale marker beds and probably reflect an increase in the low-^{87}Sr/^{86}Sr hydrothermal strontium flux associated with the emplacement of the Ontong-Java and Kerguelen plateaus (120 to 110 Ma) and the Caribbean Plateau (89 to 91 Ma). The modeled flux is consistent with the volumes and eruption rates of the oceanic plateaus but is far smaller than expected from the proposed Cretaceous crustal production rates of 50 to 100 percent greater than modern.

The strontium isotopic composition of seawater exhibits both large and small fluctuations throughout the Phanerozoic; these are attributed to changes in the riverine Sr flux controlled by orogenic uplifting and major glaciations, increased submarine volcanism and sea-floor spreading rates, and overall changes in rock exposures and eustatic sea level (*1–5*). Modeling indicates that major fluctuations are closely tied to continental deformation rates for most of the Phanerozoic except for the period from 300 to 90 Ma (*5*). During part of this period, between 125 and 90 Ma (the mid-Cretaceous), submarine volcanic activity was greater, sea level was higher, thermohaline circulation was markedly different (*6*), and ocean temperatures were warmer than present (*7*). Sedimentary rocks with high amounts of organic carbon, representing so-called "oceanic anoxic events," were deposited during discrete intervals of the mid-Cretaceous (*8–11*).

B. L. Ingram, Department of Geology and Geophysics, University of California, Berkeley, CA 94720, USA.
R. Coccioni, Instituto di Geologia, Via Santa Chiara 27, 61029 Urbino, Italy.
A. Montanari, Osservatorio Geologico di Coldigioco, 62020 Frontale di Apiro (MC), Italy.
F. M. Richter, Department of Geophysical Sciences, University of Chicago, Chicago, IL 60637, USA.

Because the $^{87}Sr/^{86}Sr$ ratio in seawater reflects a balance of Sr from continental weathering and hydrothermal sources, knowledge of Sr isotopic variations in seawater during the mid-Cretaceous may help constrain the causes for this exceptional preservation of organic carbon. For example, increased continental weathering rates would increase the flux of dissolved Sr with a high $^{87}Sr/^{86}Sr$ ratio (modern average = 0.711) and of nutrients to the oceans, causing an increase in oceanic primary productivity (*10*). Alternatively, an increase in sea-floor spreading, submarine volcanism, and hydrothermal activity would increase the flux of Sr with a low $^{87}Sr/^{86}Sr$ ratio (modern average = 0.703), as well as the flux of reducing sulfide, thereby decreasing the oxygen content in bottom water (*12, 13*). Earlier Sr isotopic data from mid-Cretaceous marine sedimentary rocks are too scattered to determine the relation between seawater Sr isotopic fluctuations and paleoceanographic and volcanogenic events (*14, 15*). In this study, we refine the mid-Cretaceous Sr isotopic curve using Sr separated from fish tooth apatite and evalu-

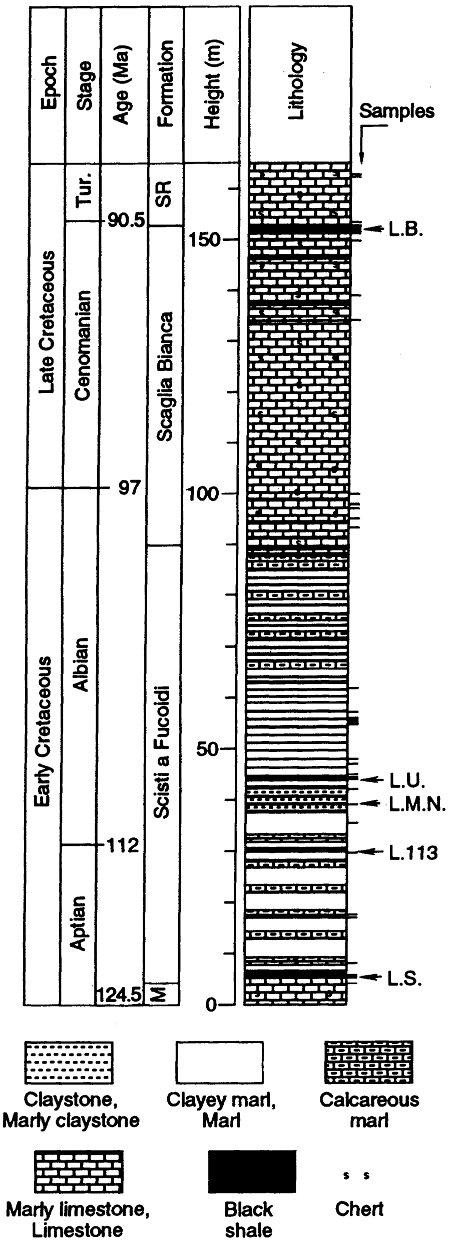

Fig. 1. Generalized stratigraphy of the mid-Cretaceous pelagic sequence in the Umbria-Marche Apennines with the locations of major anoxic events (L.B., Livello Bonarelli; L.M.N., Livello Monte Nerone; L.S., Livello Selli; L.U., Livello Urbino; and L.113, Livello 113). Tick marks on right side indicate stratigraphic level of samples. Tur, Turonian; M, Maiolica Formation; SR, Scaglia Rossa Formation.

Table 1. Stratigraphic information and isotopic results of analyses for samples used in this study (*30*).

Sample*	Age (Ma)	Planktonic foraminiferal zone†	Rb (ppm)	Sr (ppm)	$^{87}Sr/^{86}Sr$ average
SA-2B	122.86	G.m.-G.b.	1.1	3087	0.707556
SE-1	122.46	G.m.-G.b.	–	–	0.707513
SE-2	122.42	G.m.-G.b.	–	–	0.707452
SE-3	122.34	G.m.-G.b.	–	–	0.707461
SE-4	122.18	G.m.-G.b.	–	–	0.707460
SA-3	121.30	G.f.	–	–	0.707479
BO-5	117.70	G.a.	0.8	369	0.707485
BO-6	117.50	G.a.	–	–	0.707513
PLG-112	112.58	T.b.	8.5	2331	0.707349
PLG-126	111.08	H.p.	0.2	2068	0.707388
SSA-66	110.32	H.p.	–	–	0.707516
SSA-73	109.68	H.p.	–	–	0.707452
SA-2	109.25	H.p.	–	–	0.707451
PLG-177	109.14	H.r.-T.p.	–	–	0.707477
SA-7	109.03	H.r.-T.p.	1.5	2741	0.707461
PLG-197	108.60	H.r.-T.p.	–	–	0.707453
SA-40	108.38	H.r.-T.p.	5.4	1278	0.707477
PLG-252	106.95	H.r.-T.p.	–	–	0.707478
CA-23	106.88	H.r.-T.p.	1.7	2372	0.707482
CA-25A	106.84	H.r.-T.p.	–	–	0.707539
CA-26B	106.82	H.r.-T.p.	–	–	0.707594
CA-27	106.80	H.r.-T.p.	0.1	2655	0.707461
SL-3	106.71	H.r.-T.p.	4.6	1623	0.707551
FB-6	106.67	H.r.-T.p.	2.3	1867	0.707475
SL-4	106.41	H.r.-T.p.	–	–	0.707466
SL-17	105.42	H.r.-T.p.	–	–	0.707618
BO-42	98.65	R.a.-P.b.	–	–	0.707547
BO-60	98.26	R.a.-P.b.	–	–	0.707654
BO-79	97.85	R.a.-P.b.	6.6	8337	0.707524
BO-86	97.68	R.a.-P.b.	3.8	1499	0.707647
BO-86B	97.66	R.a.-P.b.	–	–	0.707494
BO-103	97.23	R.a.-P.b.	–	–	0.707571
BO-427	92.86	R.c.	2.6	2666	0.707527
FU-2.71	92.26	R.c.	1.5	6824	0.707537
FU-14.36	90.90	R.c.	0.3	5677	0.707517
VF-1	90.75	W.a.	10.7	2416	0.707449
BO-BON 1	90.74	W.a.	22.1	630	0.707533
SG-3	90.73	W.a.	0.3	1372	0.707496
VF-2	90.73	W.a.	4.1	3602	0.707488
VF-4	90.69	W.a.	2.1	5406	0.707475
ME-63	90.68	W.a.	–	–	0.707511
SG-11	90.68	W.a.	31.1	3908	0.707519
BAC-BON 2	90.66	W.a.	3.3	5835	0.707510
SG-16	90.63	W.a.	15.7	6864	0.707485
FU-17.07	90.56	W.a.	2.1	5840	0.707527
FO-6	89.35	H.h.	1.2	2051	0.707607
FO-7	89.28	H.h.	0.4	2269	0.707524

*Section abbreviations for samples located in the Umbria-Marche Apennines: SA, Santa Anna; SE and SSA, "Apechiese" Road; BO, Bottaccione; PLG, Poggio le Guaine; CA, Castraccioni; SL, Santo Lazzaro; FB, Fiume Bosso; FU, Furlo; BON, Bonarelli; ME, Meggiano; BAC, Bacciardi; for those located in the Venetian Alps: VF, Cismon; SG, Segusino-Vas; FO, first occurrence. †Abbreviations: G.m.-G.b., *Globigerinelloides maridalensis–G. blowi*; G.f., *G. ferreolensis*; G.a., *G. algerianus*; T.b., *Ticinella bejaouaensis*; H.p., *Hedbergella planispira*; H.r.-T.p., *H. risch–T. primula*; R.a.-P.b., *Rotaliporal appenninica–Planomalina buxtorfi*; R.c., *R. cushmani*; W.a., *Whiteinella archaeocretacea*; H.h., *H. helvetica*. The planktonic foraminiferal biozonation is from Sigal (*38*) using the time scale of Harland and others (*39*). The ages were determined by assigning an age of 124.5 to the *G. gottisi–G. duboisi* zone, 112 Ma to the upper part of the *T. bejaouaensis* zone, and 97 Ma to the top of the *R. apenninica–P. buxtorfi* zone and assuming constant sedimentation rates in the stratigraphic intervals between these boundaries. Continuous, cyclic sedimentation with a Milankovitch climate origin was demonstrated for the Scisti a Fucoidi (*40*) as well as in the Scaglia Bianca Formation (*41*).

ate the relation between variations in the seawater $^{87}Sr/^{86}Sr$ ratio and major paleoceanographic and volcanogenic events by modeling the Cretaceous oceanic Sr budget.

Fish teeth were separated from uppermost Barremian sedimentary rocks of the Maiolica Formation, the Aptian to upper Albian Scisti a Fucoidi Formation, and the upper Albian to lower Turonian Scaglia Bianca Formation, all exposed in the Umbria-Marche region of the northern Apennines (Italy) and in the Venetian Alps (*16*). These formations consist of rhythmically interbedded pelagic limestone and marl and of carbonate-poor shale (*17–19*) (Fig. 1). The Scisti a Fucoidi contains the Livello Selli of early Aptian age, a 1- to 3-m-thick, organic-rich regional marker bed (*19–21*) that represents a global anoxic event (*21–23*). Other regional black shale horizons in the Scisti a Fucoidi include the Livello 113, the Livello Monte Nerone, and the Livello Urbino. The top of the Scaglia Bianca Formation contains a regional organic-rich marker bed known as Livello Bonarelli, which represents a global anoxic event near the Cenomanian-Turonian boundary (*24–26*).

Fossil fish tooth apatite was chosen for Sr isotopic analyses because it may preserve the original $^{87}Sr/^{86}Sr$ ratio of seawater more reliably than carbonate, particularly in old (>50 Ma), carbonate-poor sedimentary rocks. The fish teeth consist of apatite, which is usually coated with a protective phosphate rich in rare earth elements during diagenesis and is less soluble in water than carbonate (*27*). It also contains a much higher Sr concentration than average marine calcite [1000 to 6000 parts per million (ppm) in fish tooth apatite, as compared with 600 to 1500 ppm in carbonates]. In recrystallized carbonate samples (for example, foraminiferal tests or mollusk shells), the amount of variation in the $^{87}Sr/^{86}Sr$ ratio depends on (i) the timing and rate of recrystallization, (ii) the proportion, $^{87}Sr/^{86}Sr$ ratio, and Sr content of the noncarbonate phases in the sediment, and (iii) the burial depth and temperature, including proximity to oceanic basement (*28*). If compaction and diagenesis occurred soon after deposition, as is the case in many deep-sea carbonate rocks, the $^{87}Sr/^{86}Sr$ ratio of the recrystallized carbonate would probably not be significantly different from the original ratio. However, if recrystallization is prolonged as a result of a low sedimentation rate, the $^{87}Sr/^{86}Sr$ ratio of the recrystallized carbonate may be shifted significantly from the original values (*29*).

We measured the $^{87}Sr/^{86}Sr$ ratios for 47 fish teeth samples and converted the $^{87}Sr/^{86}Sr$ ratio to a $\Delta^{87}Sr$ value by normalization to the modern seawater standard (*30*) (Table 1). We also measured Sr, Rb (Table 1), Nd, and Sm concentrations for the larger of the samples by isotope dilution (*30*). The Rb concentrations were generally less than 10 ppm, except for two samples with Rb concentrations of 22 and 31 ppm, and Sr concentrations ranged between 369 and 8337 ppm. The average Sm and Nd concentrations were 1016 and 288 ppm, respectively (*30*). We assume that minimal postdepositional recrystallization of the fossil fish teeth has occurred because of the high Sr concentrations (*31*), with the exception of four samples that had less than 1500 ppm.

The range of $\Delta^{87}Sr$ of the fish teeth is 28 (or 28×10^{-5} of the $^{87}Sr/^{86}Sr$ ratio) (Fig. 2A), much less than earlier data from foraminifers and bulk carbonates (*15*), which had a range of 60 $\Delta^{87}Sr$ units between 90 and 125 Ma (*14, 15*). In some levels with closely spaced samples, such as at 98 and 107 Ma, fluctuations in the $\Delta^{87}Sr$ occur too rapidly to reflect original seawater. Because the shale matrix that encased the fish teeth contains a high proportion of detrital clay minerals with high $^{87}Sr/^{86}Sr$ ratios, we assume that the lowest $^{87}Sr/^{86}Sr$ ratio measured in the fish teeth for any age should provide the best estimate of original seawater.

The data show that the $^{87}Sr/^{86}Sr$ ratio of seawater decreased by 8×10^{-5} to 12×10^{-5} at 124 to 121 Ma, 114 to 110 Ma, and 91 to 89 Ma. These three periods correspond, in the Apennines, to the deposition of three prominent organic-rich black shale units: the Livello 113 and Livello Selli of Aptian-Albian age (*32*), and the Livello Bonarelli of Cenomanian-Turonian age.

To determine the possible origin of these excursions, we calculated the Sr isotopic response that might be associated with periods of especially rapid oceanic crustal production or massive magmatism associated with the emplacements of large igneous provinces such as the Ontong-Java Plateau. For example, it has been proposed that from 125 to 80 Ma, oceanic crustal production rates were 50 to 100% greater than during subsequent periods (*33, 34*). Larson (*34*) estimated an increase to 30 million to 35 million km^3/year from about 20 million km^3/year during the Aptian-Albian time. The emplacement of the Ontong-Java and Manihiki plateaus in the Pacific Ocean, and the Kerguelen Plateau in the Indian Ocean, also occurred during the Aptian-Albian (*23*). The volume of the Ontong-Java Plateau has been estimated at 24 million to 65 million km^3 (*23*), corresponding to an emplacement rate between 8 and 22 km^3/year over a 3-million-year period (*23*).

The proposed increase in ocean crust

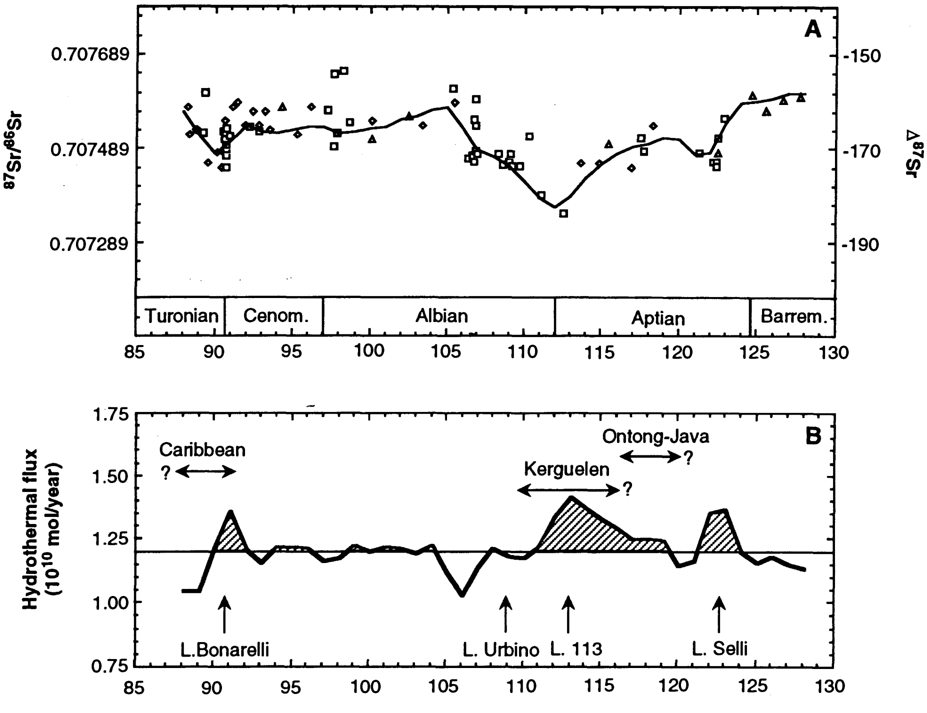

Fig. 2. (**A**) $^{87}Sr/^{86}Sr$ and $\Delta^{87}Sr$ plotted against age for fish teeth samples from the mid-Cretaceous Italian pelagic sequences (squares), along with previously published data (*15*) from Deep-Sea Drilling Project (DSDP) site 167 (triangles) and foraminiferal limestones from Iran (diamonds). Barrem., Barremian. (**B**) The calculated hydrothermal flux of Sr. Oceanic plateaus and episodes of oceanic anoxia represented by the Livello Bonarelli, Urbino, 113, and Selli are indicated. The horizontal line at 1.2×10^{10} mol/year represents the average hydrothermal flux and corresponds to the Cretaceous background level (*5*).

production, as well as the formation of the large oceanic plateaus, should have resulted in a greater rate of hydrothermal exchange of Sr, accompanied by a substantial decrease in the $^{87}Sr/^{86}Sr$ ratio of seawater. To determine the magnitude of this Sr isotopic response, we used the following equation of Sr isotopic evolution for seawater (*5*)

$$N dR_o/dt = J_r(R_r - R_o) + J_h(R_h - R_o)$$

where N is the total number of moles of Sr in the ocean; R_o, R_r, and R_h are the Sr isotopic compositions of seawater, globally averaged riverine inflow, and hydrothermal input; t is time; and J_r and J_h are the riverine and hydrothermal Sr flux in moles per year. We used as a baseline the Cretaceous Sr budget of Richter *et al.* (*5*), in which $N = 1.25 \times 10^{17}$ mol, $J_r = 2.2 \times 10^{10}$ mol/year, $R_r = 0.710$, $J_h = 1.2 \times 10^{10}$ mol/year, and $R_h = 0.703$. This hydrothermal flux value corresponds to an assumed background rate of crustal production of about 20 km^3/year. Oceanic crustal production rates and submarine volcanism in excess of this will increase the hydrothermal exchange of Sr at a rate of 6×10^8 mol/year per cubic kilometer of new volcanic material, assuming the present-day Sr exchange rate for submarine volcanic material.

We first calculated the hydrothermal Sr flux necessary to produce the observed $^{87}Sr/^{86}Sr$ ratio of seawater, assuming a constant riverine Sr flux (Fig. 2B). The average hydrothermal flux (J_h) indicated by the Sr data is 1.2×10^{10} mol/year, which is similar to the expected baseline for the Cretaceous (*5*). There are three periods where the hydrothermal Sr flux increased to 1.4×10^{10} mol/year (about 15% higher than background): at 123 to 121 Ma, 119 to 111 Ma, and 92 to 90 Ma. The area under these peaks corresponds to the total amount of hydrothermal Sr produced by the extrusive component of the Ontong-Java and Kerguelen plateaus (Fig. 2B). However, the estimated time interval of the emplacements of the Ontong-Java Plateau is 4 million years younger than the hydrothermal Sr flux peak (*23, 35*). It is difficult to compare ages with confidence because of the paucity of radiometric dating and incomplete sampling of the Ontong-Java Plateau [the Ontong-Java Plateau has been dated in only one Ocean Drilling Program (ODP) hole, and the estimated volume and emplacement rate vary by at least a factor of 3 (*23*)]. The seawater Sr isotopic composition may help constrain the magnitude and duration of the ocean plateaus.

We consider two hydrothermal flux models (Fig. 3). Changes in hydrothermal flux in the first are large and correspond to a rapid increase in crustal production rate in the early Aptian to about 35 km^3/year at about 120 Ma, followed by a linear decline back to about 20 km^3/year at 70 Ma (*33, 34*). In the second, we calculate changes in hydrothermal flux in the 120 to 110 Ma time interval, corresponding to the extrusive component of Ontong-Java and Manihiki plateaus and the Kerguelen Plateau volcanism (*35*). Comparison of the actual data to the calculated changes in the Sr isotopic composition of seawater suggests that the crustal production rates proposed by Larson (*33, 34*) are far too large (Fig. 3B). Similarly, the hydrothermal fluxes of nutrients and CO_2 linked with ocean anoxia and a greenhouse climate may also be too large. It is possible, although not likely, that an increased flux of low $^{87}Sr/^{86}Sr$, hydrothermal Sr was offset by a corresponding increase in high $^{87}Sr/^{86}Sr$ Sr by accelerated continental weathering. A large decrease in the hydrothermal exchange rate during the mid-Cretaceous would likewise explain the lack of response in the seawater $^{87}Sr/^{86}Sr$, although there is no evidence of this. In either case, we would not expect to see the Sr isotopic response to the submarine volcanogenic events seen in our Sr isotopic data.

Although our data suggest that the proposed crustal production rates of Larson (*34*) are unlikely, there is evidence in both amplitude and duration of the Sr isotopic composition in seawater for changes in the hydrothermal flux associated with the emplacement of the Ontong-Java and Kerguelen plateaus. The data are consistent with emplacement rates of extrusive rocks (*35*) of about 10 km^3 over 3 million years for the Ontong-Java Plateau and 8 km^3 in 5 million years for the Kerguelen Plateau (Fig. 3). The Sr data also indicate a rapid decrease in seawater $^{87}Sr/^{86}Sr$ (caused by an increase in hydrothermal Sr flux) between 89 and 91 Ma, coincident with the initiation of the emplacement of the Caribbean plateau basalts (*36, 37*). The decrease in seawater Sr isotopic composition recorded within the black shale horizons provides evidence for a link between mid-Cretaceous submarine volcanogenic events and increased organic carbon preservation in the sedimentary record. Other periods of low $^{87}Sr/^{86}Sr$ in Phanerozoic seawater may also be correlated with mantle plume events and oceanic anoxia. For example, a proposed mantle plume event in the Permian (*34*) correlates with the lowest $^{87}Sr/^{86}Sr$ in seawater for the entire Phanerozoic (*14*).

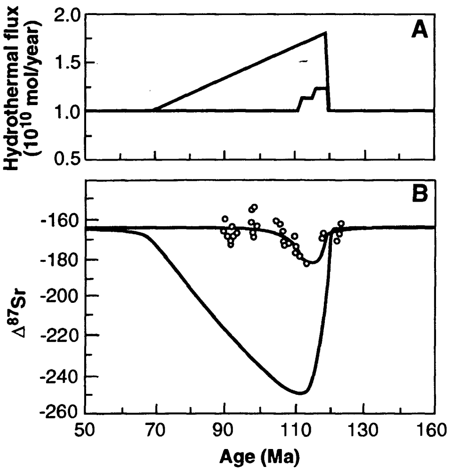

Fig. 3. (**A**) The two cases of varying hydrothermal Sr flux (fractional changes from a base value of 1.2×10^{10} mol/year) from which we have calculated seawater Sr isotopic changes. The curve with the larger change is a simplified version of the Sr flux that would accompany changes in the rate of oceanic crustal production proposed by Larson (*33, 34*), assuming that the hydrothermal exchange of Sr per cubic kilometer of new oceanic crust was the same during the Cretaceous as it is today. The smaller flux changes in volcanic rock, associated with 10×10^6 km^3 of lavas from the Ontong-Java and Manihiki plateaus followed by 8×10^6 km^3 (*35*) of lavas from the Kerguelen Plateau (*35*), are also shown. (**B**) Comparison of the calculated Sr isotopic evolution of seawater, when the only change in the Sr budget of the ocean is the hydrothermal flux (curves), to the actual measured values (circles). The solid curve with values far below the actual data is the result for the larger of the two changes in the hydrothermal flux shown in (A). The solid curve falling more nearly through the data is for the hydrothermal flux changing in response to only Ontong-Java, Manihiki, and Kerguelen volcanism.

REFERENCES AND NOTES

1. G. W. Brass, *Geochim. Cosmochim. Acta* **40**, 721 (1976).
2. D. J. DePaolo and B. L. Ingram, *Science* **227**, 938 (1985).
3. M. E. Raymo, W. F. Ruddiman, P. N. Froelich, *Geology* **16**, 649 (1988).
4. A. N. Dia, A. S. Cohen, R. K. O'Nions, N. J. Shackleton, *Nature* **356**, 786 (1992).
5. F. M. Richter, D. B. Rowley, D. J. DePaolo, *Earth Planet. Sci. Lett.* **109**, 11 (1992).
6. E. J. Barron and W. N. Washington, in *The Carbon Cycle and Atmospheric CO_2: Natural Variations Archean to Present*, E. T. Sunquist and W. S. Broecker, Eds. (Geophys. Monogr. 32, American Geophysical Union, Washington, DC, 1985), pp. 546–553.
7. S. M. Savin, *Earth Planet. Sci. Lett.* **5**, 319 (1977).
8. S. O. Schlanger and H. C. Jenkyns, *Geol. Mijnbouw.* **55**, 179 (1976).
9. M. A. Arthur, W. E. Dean, S. O. Schlanger, *AAPG Bull.* **63**, 876 (1979).
10. H. C. Jenkyns, *Geol. Soc. J.* **137**, 171 (1980).
11. M. A. Arthur, W. E. Dean, S. O. Schlanger, in (*6*), pp. 504–530.
12. J. C. G. Walker, *Mar. Geol.* **70**, 159 (1986).
13. M. A. Arthur, R. L. Larson, W. E. Dean, *Eos* **71**, 1660 (1991).
14. W. H. Burke *et al.*, *Geology* **10**, 516 (1982).
15. R. B. Koepnick *et al.*, *Chem. Geol.* **58**, 55 (1985).
16. G. Salvini, thesis, Firenze University (1993).
17. R. Coccioni *et al.*, "Fossili, Evoluzione, Ambiente," *Atti 2° Convegno Internazionale*, G. Pallini, F. Cecca, S. Cresta, M. Santantonio, Eds. (Tecnostampa, Ostra Vetere, 1990), pp. 163–201.
18. R. Coccioni, S. Galeotti, D. Ragni, 6th Annual

Meeting of the International Geological Correlation Programme No. 262, Cretaceous Facies in Orogenic Belts (Athens, Greece), p. 4 (abstr.) (1992).
19. R. Coccioni *et al.*, *Boll. Soc. Geol. Ital.* **106**, 183 (1987).
20. R. Coccioni *et al.*, in *Cretaceous of the Western Tethys*, J. Wiedmann, Ed. (Lubrecht and Cramer, Forestburgh, NY, 1990), pp. 563–584.
21. W. V. Sliter, *Geology* **17**, 909 (1989).
22. F. Robaszynski, *Geobios* **11**, 311 (1988).
23. J. A. Tarduno *et al.*, *Science* **254**, 399 (1991).
24. M. A. Arthur and I. Premoli Silva, in *Nature and Origin of Cretaceous Carbon-Rich Facies*, S. O. Schlanger and M. B. Cita, Eds. (Academic Press, New York, 1982), pp. 7–54.
25. S. O. Schlanger *et al.*, *Geol. Soc. Am. Spec. Pap.* **26**, 371 (1987).
26. M. A. Arthur, W. E. Dean, L. M. Pratt, *Nature* **335**, 714 (1988).
27. B. Schmitz, G. Aberg, L. Werdelin, P. Forey, S. V. Bendix-Almgreen, *Geol. Soc. Am. Bull.* **103**, 786 (1991).
28. F. M. Richter and D. J. DePaolo, *Earth Planet. Sci. Lett.* **83**, 27 (1987).
29. The ^{87}Sr/^{86}Sr ratios in fish teeth from a Miocene volcano-sedimentary clay in the northeastern Apennines are consistent with the bulk ratios for carbonate of adjacent limestones overlying and underlying the clay layer, whereas the ^{87}Sr/^{86}Sr ratios of recrystallized foraminiferal tests have been shifted [A. Montanari *et al.*, *Newsl. Stratigr.* **23**, 151 (1991)].
30. Each sample was composed of 2 to 10 teeth, weighing from 0.1 to 0.5 mg. The fish teeth samples were dissolved in 4 N nitric acid. One aliquot was passed through an ion exchange column to separate Sr from other elements, and the ^{87}Sr/^{86}Sr ratio measurements were made on a VG Sector-354 mass spectrometer (Fisons Instruments, United Kingdom) in dynamic multicollection mode [see B. L. Ingram, thesis, Stanford University (1992)]. Each sample was measured in duplicate. The other aliquot was spiked with ^{84}Sr, ^{85}Rb, ^{145}Nd, and ^{152}Sm to determine Sr, Rb, Nd, and Sm concentrations by isotope dilution. The Sr standards used were the U.S. Geological Survey EN-1 *Tridacna* shell for modern seawater and the NBS-987 Sr standard, with ^{87}Sr/^{86}Sr ratios of 0.709189 and 0.710275, respectively. The ^{87}Sr/^{86}Sr ratios were normalized to seawater standard as follows: $\Delta^{87}\mathrm{Sr} = (^{87}\mathrm{Sr}/^{86}\mathrm{Sr}_{\mathrm{sample}} - {}^{87}\mathrm{Sr}/^{86}\mathrm{Sr}_{\mathrm{standard}}) \times 10^5$. The uncertainty of each ^{87}Sr/^{86}Sr ratio measurement (2σ) is $\pm 1 \times 10^{-5}$, or ± 1 Δ^{87}Sr unit.
31. It has been demonstrated that postdepositional recrystallization of ancient fish teeth causes an increase in crystallinity and carbonate content and a decrease in Sr content (those samples with the highest crystallinity index had Sr concentrations below 2000 ppm). A. Shemesh, *Geochim. Cosmochim. Acta* **54**, 2433, (1990).
32. The black shale sediments are thought to be deposited during warm, greenhouse climates [H. Weissert and A. Lini, in *Controversies in Modern Geology*, D. W. Muller, J. A. McKenzie, H. Weissert, Eds. (Academic Press, New York, 1991), pp. 173–191].
33. R. L. Larson, *Geology* **19**, 547 (1991).
34. R. L. Larson, *ibid.*, p. 963.
35. M. F. Coffin and O. Eldholm, *Rev. Geophys.* **19**, 1 (1994).
36. M. A. Richards, D. L. Jones, R. A. Duncan, D. J. DePaolo, *Science* **254**, 263 (1991).
37. T. W. Donnelly, K. Melson, R. Kay, J. J. W. Rogers, *Init. Rep. Deep Sea Drill. Proj.* **15**, 989 (1973).
38. J. Sigal, *Géol. Mediterr.* **4**, 99 (1977).
39. W. B. Harland *et al.*, *A Geologic Time Scale 1989* (Cambridge Univ. Press, Cambridge, 1990), pp. 1–263.
40. T. D. Herbert and A. G. Fischer, *Nature* **321**, 739 (1986).
41. B. Beaudoin and E. M'Ban, in *Proceedings of the 29th International Geology Congress*, Kyoto, Japan, 1992 (abstr.), vol. 2/3, p. 291.
42. We thank S. C. Brassell, J. C. Ingle, M. McWilliams, Y. Kolodny, and M. Chambers for helpful reviews of the manuscript and D. J. DePaolo for use of his laboratory at the Center of Isotope Geochemistry at the University of California, Berkeley. This work was started as the doctoral thesis of B.L.I. at Stanford University and was supported by the Petroleum Research Fund (B.L.I.), the Ministero Universitario della Ricerca Scientifica e Tecnologica (MURST) of Italy (R.C.), and National Science Foundation grant EAR-91059297 and Exxon Production Research (A.M.).

17 December 1993; accepted 15 March 1994

Origin of Saturn's E Ring: Self-Sustained, Naturally

Douglas P. Hamilton* and Joseph A. Burns†‡

Saturn's diffuse E ring spans the region between 3 and 8 saturnian radii (R_S), has its peak brightness near the orbit of the satellite Enceladus (3.95 R_S), and is thought to be composed primarily of icy particles 1.0 ± 0.3 micrometers in radius. Such particles are shown to move periodically along highly elliptical paths that cross the orbits of several saturnian satellites; the resulting energetic collisions of E ring particles with embedded satellites are capable of sustaining the E ring at its current optical depth. With several reasonable assumptions, this model naturally selects Enceladus as the primary source of ring material and may also provide mechanisms that explain the generation of the unusual amount of submicrometer dust in the neighboring F and G rings, the excess of OH molecules observed within the E ring, and the orbital brightness variations of nearby satellites.

The radial distribution, radial extent, and three-dimensional structure of Saturn's E ring (*1*) are consistent with the orbital dynamics of micrometer-sized particles injected at Enceladus (*2, 3*). Such particles move along paths that periodically become highly elliptical, instead of remaining circular as typically assumed (Fig. 1).

All bodies orbiting Saturn are perturbed by the planet's significant equatorial bulge, which causes elliptical orbits to precess in space while retaining their size and shape. Micrometer-sized dust grains are additionally influenced by strong nongravitational forces, principally electromagnetism and solar radiation pressure. The former arises because objects near Saturn invariably acquire negative electric potentials by sweeping up magnetospheric electrons and ions (*2*). Movement of these charged grains through Saturn's rotating magnetic field (*4*) causes a Lorentz force (*2, 3*), the primary consequence of which is orbital regression (that is, elliptic orbits rotate in the direction opposite to that induced by oblateness; as before, the orbital size and shape are unaltered). Finally, small grains are measurably perturbed by solar radiation pressure, which is directed radially away from the sun (*5*); unlike the previously mentioned perturbations, radiation pressure induces a periodic variation in orbital eccentricity. The amplitude of this eccentricity oscillation is inversely proportional to the orbital precession rate (*2*).

When all these perturbations act simultaneously on E ring grains 1 μm in radius, precession from oblateness nearly cancels regression from the Lorentz force, allowing eccentricities to become appreciable (Fig. 2). The orbits of bigger (and smaller) particles precess (or regress) rapidly enough that radiation pressure cannot induce such large eccentricities (Fig. 2).

Because orbits transform from circles to ellipses and back again in just a few years (Fig. 2), micrometer-sized material, even if introduced on a nearly circular path, swiftly covers a broad, flattened torus (Fig. 1). The spatial distribution of grains that have undergone such orbital changes after being launched from Enceladus roughly matches (i) the observed radial profile of the E ring, (ii) the density peak centered on that satellite (*2*), and (iii) the observed vertical structure (*3*). This close correspondence between the model and reality suggests that Enceladus is the primary source of E ring material; moreover, the fit to the E ring's radial and vertical profiles is further improved if Tethys contributes additional material (*3*).

The E ring shares the region between 3 and 8 R_S with an ensemble of moons that travel along nearly circular paths (Table 1); consequently, whenever the orbits of E ring particles become moderately eccentric, they cross the paths of these satellites (Fig. 2). Given a satellite of radius R_{moon} on a low-eccentricity orbit at radial distance a_{moon}, a grain on a "crossing" orbit will strike the moon with an e-folding collisional time scale

---

Astronomy Department, Cornell University, Ithaca, NY 14853, USA.

*Present address: Max Planck Institut für Kernphysik, Heidelberg, Germany.
†Also at Theoretical and Applied Mechanics, Cornell University, Ithaca, NY 14853, USA.
‡To whom correspondence should be addressed.